Available online at www.sciencedirect.com

ScienceDirect

journal homepage: www.elsevier.com/locate/he

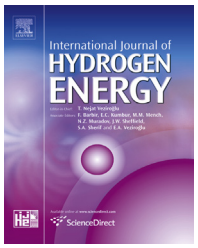

Influence of Ni to Co ratio supported on ZrO_2 catalysts in phenol steam reforming for hydrogen production

Walid Nabgan [a,b], Tuan Amran Tuan Abdullah [a,b,*], Ramli Mat [b], Bahador Nabgan [a,b], Yahya Gambo [b], Sugeng Triwahyono [c]

[a] Centre of Hydrogen Energy, Institute of Future Energy, Universiti Teknologi Malaysia, 81310 UTM Skudai, Johor, Malaysia

[b] Department of Chemical Engineering, Universiti Teknologi Malaysia, 81310 UTM Skudai, Johor, Malaysia

[c] Centre for Sustainable Nanomaterials (CSNano), Department of Chemistry, Universiti Teknologi Malaysia, 81310 UTM Skudai, Johor, Malaysia

ARTICLE INFO

Article history:
Received 12 July 2016
Received in revised form
26 September 2016
Accepted 12 October 2016
Available online 27 October 2016

Keywords:
Ni to Co ratio
ZrO_2
Phenol steam reforming
Hydrogen production

ABSTRACT

In this work, catalytic steam reforming of phenol for hydrogen production was investigated. This study focuses on the effects of Ni to Co ratio supported on ZrO_2 catalysts. The Ni_xCo_y/ZrO_2 (x = 0, 1, 2, 3, 4 where x + y = 4) catalysts were prepared by impregnation method. Steam reforming activity was tested in a fixed bed reactor at 600 °C using a feed of phenol/water mixture at a molar ratio of 1:9 and a constant liquid feed rate of 0.36 ml/min. The catalysts were characterized by BET surface area, X-ray diffraction (XRD), transmission electron microscopy (TEM), NH_3 Temperature-Programmed Desorption (NH_3-TPD), CO_2 Temperature-Programmed Desorption (CO_2-TPD), H_2 Temperature-Programmed Reduction (H_2-TPR) and thermo-gravimetric analysis (TGA). The increase in the Co content from 0 to 4, caused a decrease in the crystal size, the t-ZrO_2 phase and the reducibility of the catalysts. However, it only slightly affected the total surface area. It was found that metallic Ni_4 and Co_4 catalysts have lower activity towards phenol steam reforming and deposit higher coke due to having higher acidity sites compare to bimetallic catalysts. In contrast, Ni_3Co_1 displayed a superior catalytic activity among all the catalysts, suggesting the presence of the highest basic site and high coking resistance. Phenol conversion of 53.5% and hydrogen yield of 50.4% were achieved with the Ni_3Co_1 catalyst, even though its activity decreased by increasing the cobalt content.

Introduction

Global climate changes associated with the emission of greenhouse gases, and the reduction of natural fossil-fuel resources have attracted great concern around the world [1,2]. It is urgent to decrease the emission of greenhouse gases for environmental protection. Hydrogen is considered as a clean and environmentally friendly energy carrier. Therefore, it stands a better candidature as an energy technology in the

* *Corresponding author*. Centre of Hydrogen Energy, Institute of Future Energy, Universiti Teknologi Malaysia, 81310 UTM Skudai, Johor, Malaysia.
E-mail address: tamran@cheme.utm.my (T.A. Tuan Abdullah).

http://dx.doi.org/10.1016/j.ijhydene.2016.10.055

future global energy scenario [3–5]. Currently, hydrogen production is mainly through steam reforming of fossil fuels, which are primarily composed of natural gas, coal, and naphtha [6]. These non-renewable sources are not friendly due to the high emission of CO_2, SO_2, and NO_x gases as a result of the combustion of the fossil fuels [7]. A clean renewable fuel produced from bio-oil derivative components has attracted great interest [8].

Phenolic compounds are the major component of a bio-oil (up to 30%) [9]. The steam reforming of phenol can reduce CO_x which are the main greenhouse gases [10–12]. The reaction product of biomass pyrolysis typically contains a high molecular weight of hydrocarbon, phenolic compounds, acid, and water. Phenol was further recognized as the main component of tar formed following wood biomass gasification by steam in a fluidized bed reactor in the low-temperature range (600–700 °C) [12–14]. Phenol also can be obtained from industrial wastewater and is considered as toxic waste for many aquatic organisms. Due to its high solubility in water, it can directly convert to highly valuable gas hydrogen via catalytic steam reforming. The steam reforming of phenol, Reaction (1) and water gas shift reaction, Reaction (2) [15,16], are two major side reactions that contribute to the deposition of carbon on the catalyst surface. These lead to deactivation of the catalysts and subsequently plugged the catalyst bed [17]:

$$C_6H_5OH + 5H_2O \rightarrow 6CO + 8H_2 \quad \Delta H^o = 710.91\ kJ/mol \tag{1}$$

$$CO + H_2O \leftrightarrow CO_2 + H_2 \quad \Delta H^o = -41.15\ kJ/mol \tag{2}$$

However, one of the major problems in the phenol steam reforming is the high-potential formation of some by-products such as carbon [17–19]. This carbon formation will lead to catalyst deactivation and can make troubles for continuous steam reforming process and sustainable production of hydrogen.

Many typical active metals such as Ni [18,20], Rh [21,22], Fe [17], Rh-Fe [14], CaO [23], Pt, Pd, and Rh [24] over metal oxide supports such as γ-Al_2O_3 [20,24,25], La_2O_3 [18,22,25,26], ZrO_2 [14,18,21,22,24], MgO [14,17,21], and CeO_2 [14,17,18,21,22,24] has been studied in terms of phenol reformation. Catalysts containing a noble metal such as Ru show good stability towards coke deposition and high activity for the phenol steam reforming reaction [13,19,21,22,27,28]. However they suffer the disadvantage of having low availability and high cost, which make them not economically competitive in comparison with other transition metals based materials [29]. As a result, great potential lies in the development of an active, carbon-resistant transition metal catalyst, which is capable promoting enhanced hydrogen production via phenol steam reforming. Ni-based catalysts with a high activity for the steam reforming process have been investigated extensively in recent years [12,18,30]. Moreover, Ni has exhibited strong ability in cleavage of C–C, O–H, and C–H bonds [31]. From the industrial standpoint, it is more practical to develop Ni-based catalysts because of their low price and wide availability [32]. However, they are prone to deactivation, mainly by carbon deposition [30]. Therefore, it is highly desirable for exploring stable and active Ni-based reforming catalysts. Many efforts have been made to improve the carbon deposition resistance of the Ni-based catalysts in other feeds such methane [33,34], ethanol [35] glycerol [36], acetic acid [37,38] etc. Some reports indicated that the addition of cobalt to nickel catalysts reduces coke formation during reaction [39–48]. The integrity of the surface nickel ensembles will be broken by adding of cobalt to the nickel catalysts. This causes a decrease in the amount of nickel particle size and consequently, reduces the carbon formation [41]. Zhao et al. [49] used Ni–Co/Al_2O_3 catalyst for steam reforming of ethanol. They found that the ethanol conversion on Ni–Co/Al_2O_3 catalyst was 68.7% at 350 °C, corresponding to the metal species dispersion data 31.5%. They stated that higher dispersed catalyst exhibited higher anti-coking properties and stabilities. In our previous research [38], we found that the bimetallic Ni–Co/La_2O_3 gives the maximum acetic acid conversion and hydrogen production.

Furthermore, the metal-support interaction plays important roles in carbon deposition over supported metal catalysts during the reforming reaction. ZrO_2 as a support for Ni-based reforming catalysts has attracted interest towards strengthening the metal support interaction. This is due to its unique acidic and basic properties as well as reducing and oxidizing abilities [50]. Zirconia, not only gave rise to an exclusive kind of interaction between the active phase and support but also displayed more chemical inertness than other classical supports. Zirconia has attracted increasing attention both as catalyst support material and catalysts in a variety of catalyst systems because of its high chemical stability and redox properties, as well as the acidic and basic character of its surface hydroxyl groups [51]. In general, ZrO_2 exists in three different polymorphs at ambient pressures: monoclinic (m-ZrO_2), tetragonal (t-ZrO_2), and cubic (c-ZrO_2). The t-ZrO_2 phase shows higher stability, performance and metal dispersion for chemical reactions [31,50,52].

There is, however, a lack of systematic studies of catalyst deactivation on phenol steam reforming for hydrogen production. The present work aims to explore the influence of Ni to Co ratio supported on ZrO_2 catalysts in phenol steam reforming for hydrogen production. Catalysts with various Ni–Co contents were prepared by the incipient wetness impregnation method. Phenol was mixed with steam in a molar ratio of 1–9. In order to clarify the relationship between catalytic performance and the catalyst structural properties, the Ni_x–Co_y/ZrO_2 (x = 0, 1, 2, 3, 4 where x + y = 4) catalysts were characterized extensively using the techniques of XRD, BET, TPR, TPD-CO_2, TPD-NH_3, TEM and TGA. In addition, the kinetic study of phenol steam reforming for Ni_x–Co_y/ZrO_2 has also been discussed.

Experimental

Catalyst preparation

Cobalt and nickel supported on zirconia (all components from Aldrich) were prepared using the impregnation technique. The advantage of impregnation method is that it produces a high concentration of the active materials on the catalyst surface [53]. The procedure of this method was reported by

Athanasios et al. [54]. The weight percent compositions of the catalysts are displayed in Table 1.

The mix was heated up to 90 °C and held until it turned into a highly viscous paste. The paste was dried at 110 °C overnight in an oven. The catalysts were calcined at 750 °C for three hours. Subsequently, the catalysts were pelletized and sieved on two layers of 35 and 34 mesh to obtain particles size between 1.0 mm and 1.4 mm.

Catalyst characterization

The BET method to the isotherms of N_2 adsorption would be applied for the catalyst specific surface area calculation, measured at a temperature of liquid nitrogen on a Micromeritics Gemini 2360. Multiple point absorptions was used.

The crystalline structure of the reduced catalyst was determined by X-ray diffraction (High-Resolution X-Ray Diffractometer brand Bruker D8 Advance) using a Cu Kα radiation at 40 kV and 30 mA. Diffraction angles was measured in steps of 0.02°, at 1 s/step in the range of 20–80 (2θ). The size of the metal crystallites was calculated from line broadening with the help of the Scherrer equation. The total surface area of catalysts was measured using the multipoint BET-N_2 on a surface area analyzer, Micromeritics, Gemini 2360. Prior to the analysis, the samples were degassed at 200 °C for 2 h to remove unwanted components on the surface before outgassing the samples. Morphologies and properties of the metal particles on catalysts were obtained by JEM-2100 transmission electron microscopy (TEM) instrument operated at 200 kV.

A chemisorption analyser, Micromeritics Chemisorb 2720, was used to evaluate the reducibility of the active metals (nickel and cobalt) on the support by applying a temperature-programmed reduction of hydrogen (TPR-H_2). Before the reduction, 25 mg of the catalyst was treated at 300 °C under high purity 99.99% helium with the flow rate of 20 ml/min for an hour to remove moisture and other gas impurities. The TPR-H_2 profile was obtained by ramping the temperature at 10 °C/min, 20 ml/min of 10% (vol.) H_2/Ar between 50 °C and 800 °C.

The same apparatus, Micromeritics Chemisorb 2720 Chemisorption was used for CO_2-TPD. Prior to adsorption, to remove the adsorbed impurities completely, 35 mg of the sample was kept under 30 ml/min of argon flow rate at 600 °C, for 60 min, then cooled down to 25 °C and kept under 20 ml/min of helium flow rate for 30 min. The CO_2 saturation of the catalyst was carried out for 30 min of CO_2 flowing at 20 ml/min. A 10 °C/min linear heating rate in the temperature range of 50–800 °C was used for the CO_2 desorption. A similar method was applied for TPD-NH_3 except that the adsorbate gas was 5% NH_3 in Argon.

Thermogravimetric analysis (TGA) profiles were carried out in Perkin Elmer TGA instrument operated under nitrogen flowing in the heating rate of 10 °C/min. Exothermic weight loss was observed at the temperature range between 30 and 950 °C. This can be assigned to the combustion of deposited carbon, and the amount of coke deposited on the catalyst surface was measured by the amount of CO_2 formed during the steam reforming.

Table 1 – Ratio and weight percentage of metals in the catalyst.

Catalysts' symbol ratio	Nickel (wt.%)[a]	Cobalt (wt.%)[a]	ZrO_2 (wt.%)
Ni_4	9.98	0	90
Ni_3Co_1	7.48	2.51	90
Ni_2Co_2	4.96	4.96	90
Ni_1Co_3	2.48	7.56	90
Co_4	0	9.99	90

[a] The metal content was measured by ICP test.

Activity test

Activity tests were performed using 0.2 g of catalyst. The catalyst bed was placed in a 0.5-inch OD quartz tubular reactor with a coaxially centred thermocouple. Prior to reaction, the catalyst's bed was flushed with nitrogen at 300 °C, followed by a reduction in situ at 600 °C for 1 h with 30 ml/min of pure hydrogen. Phenol and water were fed independently into the pre-heater by means of HPLC pump (Bio-Rad$_{TM}$, Series 1350) with 0.36 ml/min before mixing with carrier N_2. The reduced samples were tested for steam reforming of phenol (H_2O/phenol (mol/mol) = 10) at atmospheric pressure. The reaction was maintained for 6 h in order to check if there was any deactivation of the catalysts. The reaction products were analysed on-line by GC with TCD (Agilent 6890N) equipped with Carboxen Plot 1010 capillary column (Fused Silica, 30 m × 0.53 mm) connected in series, using argon as a carrier gas. Meanwhile, the liquid product was analysed using a GC-FID (HP 5890 Series II) and a 0.53 mm × 30 m Db-Wax capillary column. The flow diagram of this work is shown in Fig. 1. Equations (3) and (4) were applied to compute the phenol conversion and the product (X: H_2 (or) CO (or) CO_2) yield.

$$\text{Conversion}\ (\%) = \frac{[\text{feed}]_{in} - [\text{feed}]_{out}}{[\text{feed}]_{in}} \times 100\% \quad (3)$$

$$\text{X yield}\ (\%) = \frac{\text{moles of X obtained}}{\text{moles of X obtained from stochiometric potential}} \times 100 \quad (4)$$

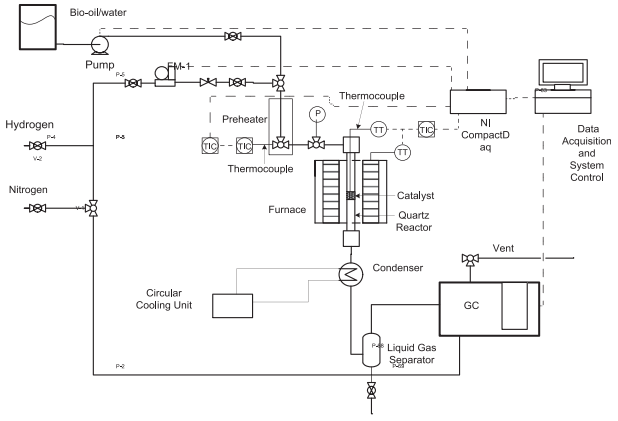

Fig. 1 – Schematic representation of the experimental setup.

Results

Characterization of the fresh catalysts

Table 2 shows the BET specific surface areas of the Ni_xCo_y/ZrO_2 (x = 0, 1, 2, 3, 4 where x + y = 4) catalysts after calcination at 750 °C. The values range between 57.9 and 66.3 m^2/g, with insignificant differences. The surface area follows the order $Ni_4 > Ni_3Co_1 > Co_4 > Ni_1Co_3 > Ni_2Co_2$. Previous research [55,56] revealed that the BET area did not follow a significant diminishing trend when the Ni content is increased.

XRD analysis was used to identify crystal phases of the catalysts. The XRD patterns of the Ni_xCo_y/ZrO_2 (x = 0, 1, 2, 3, 4 where x + y = 4) catalysts after reduction at 600 °C are displayed in Fig. 2. The XRD spectrum was characterized by several intense peaks between the diffraction angles of 20 and 80°. The XRD pattern of the Ni_xCo_y/ZrO_2 catalysts contains Bragg peaks at around 2θ = 44.52° which correspond to metallic Ni°. This can be attributed the presence of the cubic [JCPDS 45-1027] structure of Ni° and is in agreement with the previous researches [20,38,57,58]. The diffraction peaks at 2θ = 44.37° is corresponding to metallic Co° [JCPDS 01-1254], similar to reports from previous works [59] and [60]. It can be inferred that NiO and CoO were reduced at 600 °C to metallic Ni° [61,62] and metallic Co° [63], respectively. As shown in Table 2, the range of the particle size is in the magnitude of 80.4 and 44.6 nm corresponding to the sizes of Ni_4 and Co_4 catalysts respectively. The relative intensity of XRD peaks of the supported catalysts depends on the nature of the metal oxide precursors formed during the calcination step [64]. In all the Ni_xCo_y/ZrO_2 catalysts, an increase in the Ni content shifted the peaks to higher 2θ values. As a result, the only single peak was detected. This reveals that the bimetallic Ni–Co is formed during the reduction [64]. The XRD patterns of the ZrO_2 support resulted in a number of peaks located at 2θ of 24.47, 28.19, 31.48, 34.45, 40.73, 50.61, 55.62, 58.3, 60.02, 62.83, 69.67, 71.29° corresponding to (111), (200), (210), (211), (300), (320), (400), (410), (411), (331), (332) and (422) crystal planes, which can be attributed to the monoclinic ZrO_2 (m-ZrO_2) and tetragonal ZrO_2 (t-ZrO_2) [JCPDS 83-0943] structure of the ZrO_2. This is in conformity with previous research works [50,65–67].

To have better insights into the nature of the cobalt and nickel phases, TPR-H_2 of the calcined catalysts was carried out. This helped to explore the level of reduction of the Co and Ni oxide's species. The total consumptions of hydrogen for all catalysts were summarized in Table 2. Fig. 3 shows that only single reduction zones were observed. This corresponds to the area below 400 °C (~280–450 °C), corresponding to the reduction of NiO [68,69] and CoO [4,70,71] particles with weak metal-support interaction. Thus, the reduction of the NiO and CoO to metallic Ni° and Co° agrees with the XRD analysis. In particular, the reductions were peaks shifted to higher temperatures as the Co content in the catalysts increase. It suggests that higher temperatures are needed in order to reduce the cobalt oxides (>452 °C) completely as compared to nickel oxides [72]. Therefore, these catalysts were reduced at 600 °C. Additionally, the total peak area of the TPR profile presented in Table 2 shows that the reducibility of the catalysts decreased with increasing Co content. This suggests that the Co catalyst's species are more difficult to be reduced.

The corresponding CO_2 desorption profiles of the catalysts after reduction at 600 °C are displayed Fig. 4. The figure shows that the TPD-CO_2 desorption curve of the Ni_3Co_1 exhibited two

Table 2 – Total surface area and H_2 consumption of Ni_xCo_y (x = 0, 1, 2, 3, 4) supported on ZrO_2 catalysts.

Catalysts	BET-N_2 surface area (m^2/g)	H_2 consumption (μmol/g)
Ni_4	66	954.8
Ni_3Co_1	65	850.4
Ni_2Co_2	58	730.2
Ni_1Co_3	62	578.0
Co_4	64	516.3

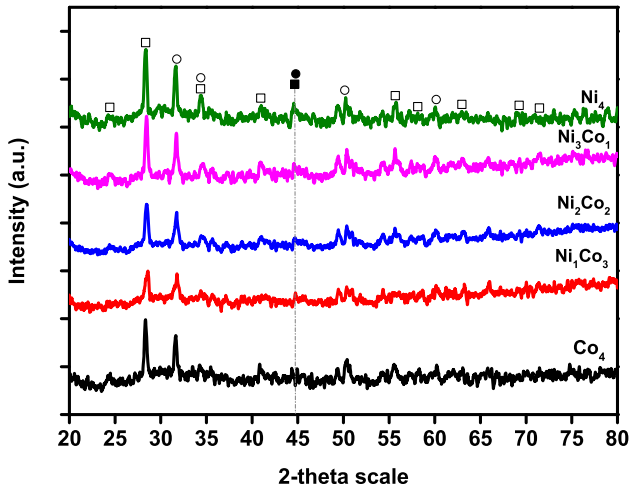

Fig. 2 – XRD pattern for Ni_xCo_y/ZrO_2 catalysts (x = 0, 1, 2, 3, 4 and x + y = 4) after reduction at 600 °C; (●) peaks correspond to metallic Ni°, (■) peaks correspond to metallic Co°, (▫) peaks correspond to monoclinic phase of ZrO_2 (m-ZrO_2) and (○) peaks correspond to tetragonal phase of ZrO_2 (t-ZrO_2).

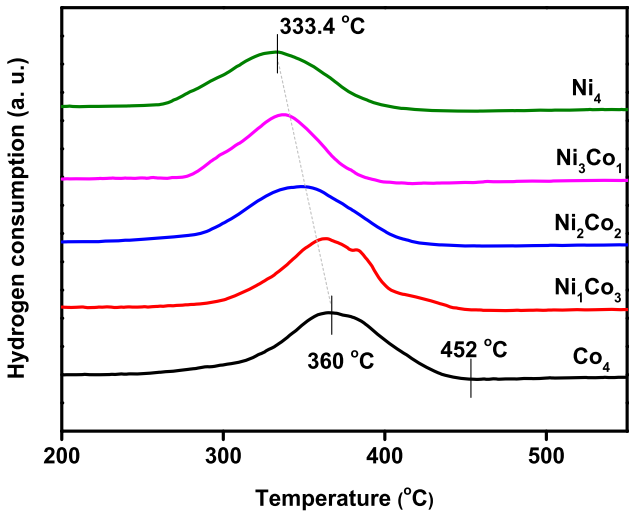

Fig. 3 – TPR-H_2 profile for the Ni_xCo_y/ZrO_2 catalysts (x = 0, 1, 2, 3, 4 and x + y = 4).

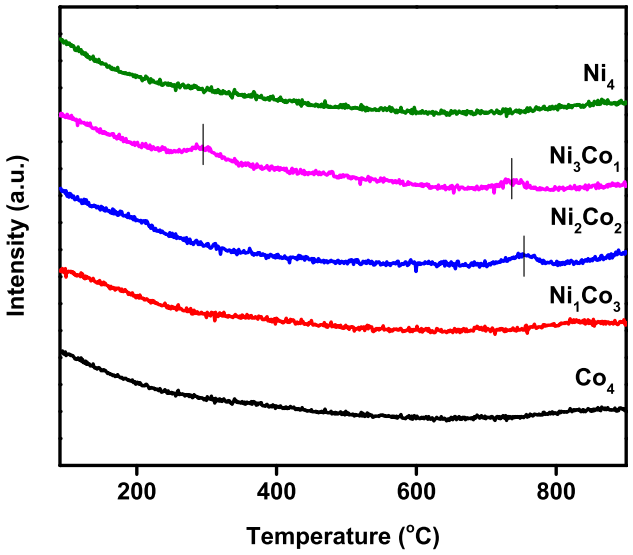

Fig. 4 – TPD-CO_2 profile of supported Ni_xCo_y/ZrO_2 (x = 0, 1, 2, 3, 4 and x + y = 4) catalysts and bare ZrO_2.

desorption small shoulder peaks centred at 293.6 and 739.2 °C. These two peaks were attributed to weak and strong basic sites, as inferred from results reported in the literature concerning the basicity of reduced Ni-based catalysts [73]. For the three catalysts, Ni_4, Ni_1Co_3, and Co_4 there were no peaks detected, which means the basicity of these samples was very low. On the other hand, Ni_2Co_2 catalyst displayed a single desorption peak with a maximum at 752.1 °C attributed to the strong basic site. It can be seen that Ni_2Co_2 desorption peak shifted to higher temperature compared to the Ni_3Co_1 catalyst. It indicates that Co° species on the ZrO_2 surface were more difficult to be oxidised by CO_2 than Ni°.

The acid properties of the catalysts involved in the present study investigated via the TPD–NH_3 technique is shown in Fig. 5. The acid site distributions are mainly classified by temperature range as weak (<250 °C), medium (250–400 °C) and strong (>400 °C) acidic sites [74]. All tested samples showed different acid site curves. For the Ni_3Co_1, Ni_2Co_2 and Ni_1Co_3 catalysts, there were no peaks observed but only very small shoulders at 250 °C, 250 °C, and 600 °C respectively. It can be seen that within the Co_4 and Ni_4 catalysts, the number of strong acid sites increased simultaneously. For the Ni_4 catalyst, two peaks between 490 and 620 °C were observed. This indicates that there was a remarkable difference in acid strength for the concerned Ni_4 catalyst. For the Co_4, there was only a single peak which appears at 190 °C. This corresponds to the weak acid site. From the TPD-NH_3 profile, it shows that the bimetallic Ni_3Co_1 and Ni_2Co_2 catalysts neutralized the acidity, but Ni_4 and Co_4 can help the acid properties of the catalysts.

Catalytic activity testing

Fig. 6 shows, the phenol conversion and the product gas yield as a function of Ni–Co ratio over zirconia. The experimental data were carried out at 600 °C, 0.2 g catalyst, and 0.36 ml/min feed flow rate. In general, the order of the catalyst's activity (in terms of phenol conversion) was found to be Ni_3Co_1 > Ni_2Co_2 > Ni_1Co_3 > Co_4 > Ni_4. Alaric et al. [72] used bimetallic Ni–Co catalysts supported on $CaAl_2O_4/Al_2O_3$ for partial oxidation of methane. They found that Ni_2Co catalyst has superior activity towards methane conversion, as well as CO and H_2 selectivity. However, they had lower stability compared to other ratios of Ni and Co. Moreover, studies by Nianjun et al. [71] used Ni_xCo_y/Al_2O_3 catalysts to investigate the activity of glycerin liquid reforming. They revealed that Ni_1Co_3 and Ni_1Co_5 catalysts were confirmed to own excellent hydrogen selectivity. They noticed that increase in Co content (for Ni_1Co_5 catalyst) results in maximum H_2 and minimum CH_4 production. They mentioned that low content of Ni is unfavourable for carbon–carbon breaking for the production of CO_2 during the reforming process. Consequently, the performance of this process was lowered. In our present study, Ni_3Co_1 was observed to have better activity as

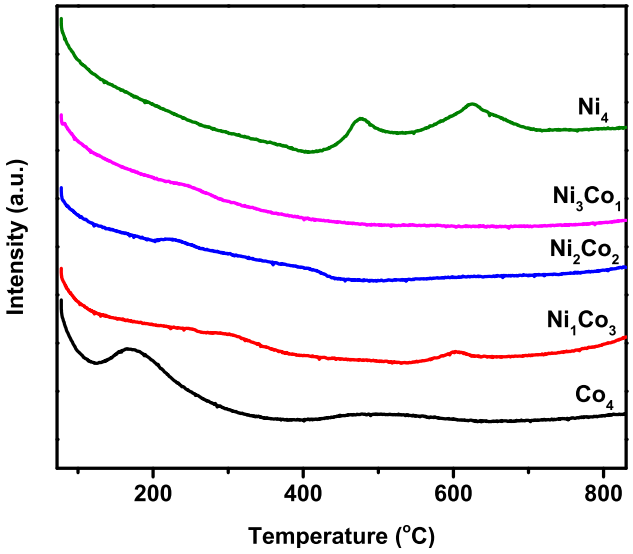

Fig. 5 – TPD-NH_3 profile of Ni_xCo_y/ZrO_2 (x = 0, 1, 2, 3, 4 and x + y = 4) catalysts and bare ZrO_2.

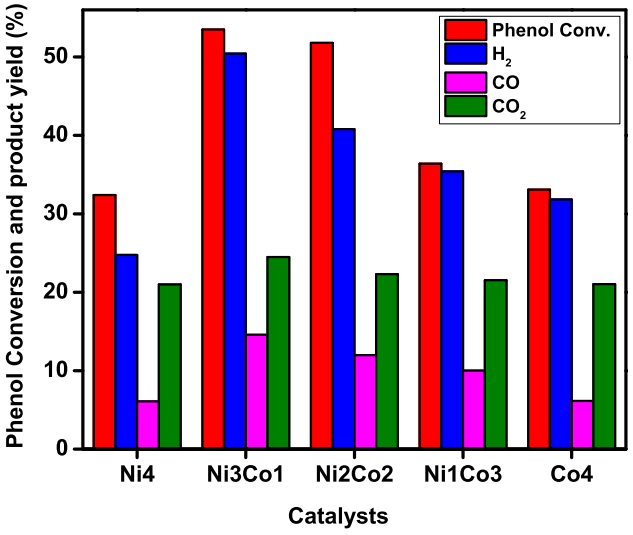

Fig. 6 – Effect of Ni_xCo_y/ZrO_2 (x = 0, 1, 2, 3, 4 and x + y = 4) catalysts on phenol conversion and product yield.

compared with other catalysts. Increase in the Co content in the Ni_xCo_y catalysts beyond 25% (Ni_3Co_1), obviously decreased the catalytic performance in all the samples investigated. This decrease can be related to the structural properties of the Ni_xCo_y catalysts such as acidity and basicity (Figs. 4 and 5). From the XRD and TPR analysis previously, the addition of Co decreased the amount of the hydrogen consumption. The phenol conversion and hydrogen yield for Ni_4 catalyst were 32.4% and 24.8% respectively. This confirms that the metallic Ni^o was the active site for the steam reforming reaction. Better performance in the catalytic activity of the catalyst was noticed with the increase in the amount of Co (Ni_3Co_1 and Ni_2Co_2 catalysts). From Fig. 6, it can be seen that the highest phenol conversion was achieved with Ni_3Co_1 and Ni_2Co_2 catalysts. The results can be attributed to the basicity of the two samples compared to other samples. It can be observed that the H_2 yield slightly decreases as Co content increases as depicted in N_3Co_1 to Co_4 catalysts. For the N_3Co_1 sample, the hydrogen yield was 50.4%, which decreased to 31.8% at the Co_4 catalyst. Besides, CO and CO_2 yield slightly decreased by increasing the cobalt content in the catalyst. CO yield decreased from 14.6% to 6.1% and CO_2 yield from 24.5% to 21% once cobalt content in the catalyst increased in N_3Co_1 to Co_4 catalysts. Decrease in CO and CO_2 yield might be attributed to the occurrence of the water–gas shift reaction (WGS: $CO + H_2O \leftrightarrow CO_2 + H_2$). The metallic Co^o particle (as shown in XRD analysis) might be less active for reforming reaction [64], due to its lowest activity and lowest phenol conversion. According to a study by Len et al. [75] on methane Oxy-CO_2 reforming, the poor activity of high content of Co in the catalyst might be due to oxidation of the Co catalyst during the reforming process. Increasing the Co content in the catalysts, the amount of t-ZrO_2 phases (which has higher stability, performance and metal dispersion than m-ZrO_2 [31,50,52]) decreased and consequently, led to lower steam reforming activity.

The effect of the time-on-stream (TOS) behaviour of the Ni_xCo_y/ZrO_2 (x = 0, 1, 2, 3, 4 and x + y = 4) catalyst on phenol steam reforming was investigated for a period of time (6 h) to further examine the catalyst deactivation. The phenol conversion and gas product yield as a function of time can be seen in Fig. 7. The experimental data were carried out at 600 °C, 0.2 g catalyst, and 0.36 ml/min feed flow rate. As it is shown in Fig. 7, for 6 h time on stream, no appreciated variation was observed in phenol conversion and H_2 and CO yield for Ni_2Co_2 and Ni_3Co_1 catalysts. Thus, the stability and activity of the catalyst remained almost constant for these two catalysts for 6 h time-on-stream. The phenol conversion and the H_2 and CO yield decreased slowly with time for Ni_4 and Co_4 catalysts. On the other hand, the CO_2 yield gradually increased with time for all the catalysts. In an overall, we can conclude that Ni_3Co_1 catalyst has the most activity, and stability compare to other catalysts.

Fig. 8 shows the plots of the dependence of activity hydrogen yield upon surface area of catalysts the hydrogen uptake capacity. The results showed a direct correlation between hydrogen uptake and the activity of Ni_xCo_y/ZrO_2 catalysts in phenol steam reforming reaction at 600 °C. As it seen in the Figure, the ratio of hydrogen yield to hydrogen uptake capacity did not change much for any of the Ni_xCo_y/ZrO_2 catalysts, indicating that the activity of Ni_xCo_y/ZrO_2 catalysts is clearly correlated with the number of hydrogen uptake on Ni_xCo_y/ZrO_2 catalysts.

As one of the most important factors in catalysis, metal particle morphology and size distribution which have great effects on catalytic activity. In this work, the sizes and

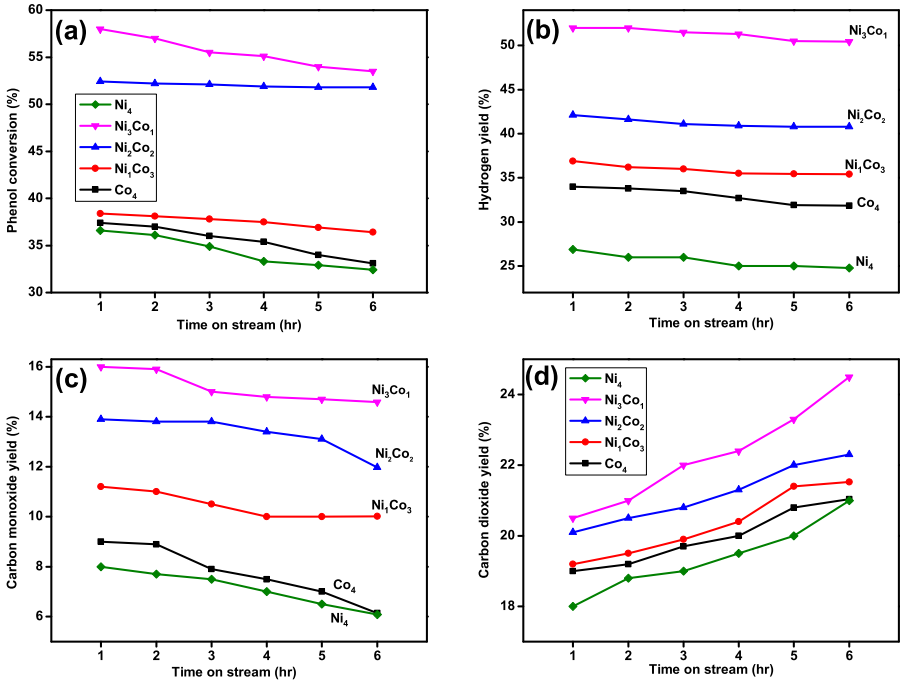

Fig. 7 – Effect of time on stream (TOS) on (a) phenol conversion, (b) hydrogen yield, (c) carbon monoxide yield, and (d) carbon dioxide yield.

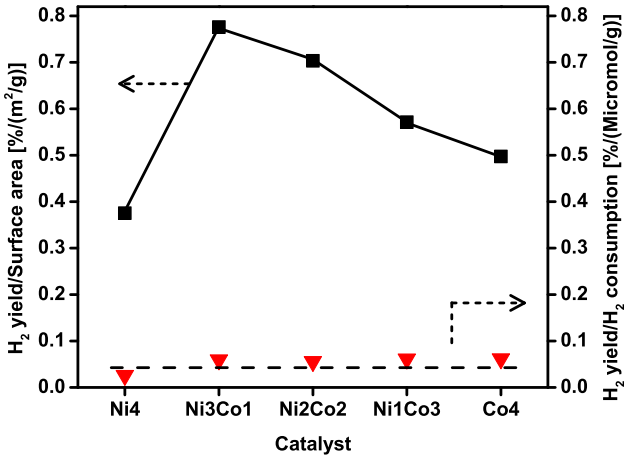

Fig. 8 – Hydrogen uptake and surface area dependences of the hydrogen yield product of phenol steam reforming reaction for Ni_xCo_y/ZrO_2 (x = 0, 1, 2, 3, 4 and x + y = 4) catalysts.

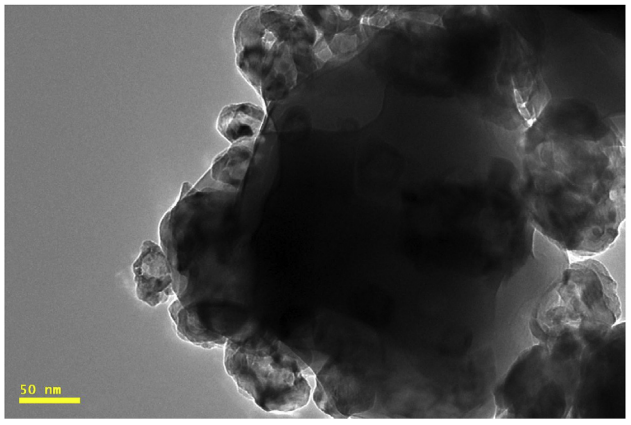

Fig. 9 – TEM image of reduced Ni_3Co_1/ZrO_2 (before reaction).

dispersions of Ni and Co particles on Ni_3Co_1/ZrO_2 catalyst (which had the best activity toward hydrogen production and phenol conversion) could be obtained in TEM images (Fig. 9). The micrographs show the irregular succession of the atomic planes corresponding to the different planes of the Ni_3Co_1/ZrO_2 lattice. The bright field TEM image of the Ni_3Co_1/ZrO_2 catalyst shows good dispersion of the metal-containing particles. Isolated crystals (crystal size ~50–100 nm) of formed Ni/Co particles can be found along with smaller metal particles of mainly ZrO_2 supported. The metal particles were segregated well from each other and suffered no sintering.

Coke analysis

The changes occurring during the steam reforming of catalysts were studied through thermo-gravimetric analyses (TGA) of the used catalysts and shows in Fig. 10. Table 3 shows the quantification of weight loss during the phenol steam reforming for Ni_xCo_y (x = 0, 1, 2, 3, 4 where x + y = 4) catalysts supported on ZrO_2. They had different amount

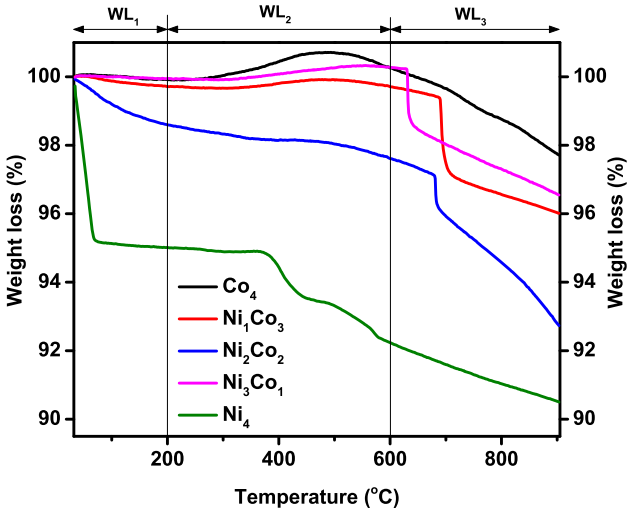

Fig. 10 – TGA profile of Ni_xCo_y/ZrO_2 (x = 0, 1, 2, 3, 4 where x + y = 4) catalysts.

Table 3 – Weight loss and amount of coke formation on the spent catalysts.

Catalysts	Weight loss (%)			Total weight loss (%)
	WL_1	WL_2	WL_3	
Ni_4	4.99	2.78	1.73	9.50
Ni_3Co_1	0.05	0	3.40	3.45
Ni_2Co_2	1.40	0.99	4.88	7.27
Ni_1Co_3	0.29	0.01	3.70	4
Co_4	0.08	0	2.21	2.29

corresponding to the weight loss associated with decomposition/oxidation of graphic from the catalyst. However in general, these data show the presence of a significant carbon deposit. The carbon deposits types were known subject on carbon oxidation temperature. In Fig. 10, the curves of weight loss as a function of temperature can be divided into three parts: below 200 °C (WL_1), 200–600 °C (WL_2) and above 600 °C (WL_3). In literature, the region bellows 200 °C have been attributed to the water and moisture evaporation. The weight loses between 200 and 600 °C have been ascribed to less stable deposits [76], whereas the weight loss above 600 °C is generally attributive to oxidation of coke deposits with the more stable [76] and/or different degree of graphitization [77]. It can be seen that from the WL_1 region the maximum weight loss (4.99%) recorded for Ni_4 catalyst due to water and moisture desorption. It can be observed that the increasing the Co content in the catalyst would avoid the adsorption of water and moisture on the catalyst surface. The WL_2 region illustrates that the weight loss of the Ni_4 is the maximum followed by Ni_2Co_2 and weight loss of Ni_1Co_3 is negligible, but some precursor residues were still present (0.01%). The TGA result shows that the Co and the Ni_3Co_1 catalysts did not suffer from coke formation on their surface in WL_1 and WL_2 regions. These two catalyst's profile exhibited additional weight gained, this might due to the oxidation of the metallic active sites [78,79]. The maximum weight loss (9.5%) was corresponding to Ni_4 catalyst.

Conclusion

In conclusion, the ratio of nickel and cobalt directly affects the activity of phenol steam reforming. Even though nickel catalysts were subjected to deactivation due to a high level of coking, yet they displayed an excellent activity and selectivity for this reaction. Ni_3Co_1 bimetallic catalyst supported on ZrO_2 was found to be highly active in the catalytic steam reforming of phenol. The presence of t-ZrO_2 phase structure and basic properties of Ni_3Co_1 directly affected the activity of the catalyst. Increase in Co content beyond 25% (as in Ni_2Co_2, Ni_1Co_3 and Co_4 catalysts) caused a decrease in the basic sites, a decrease in the catalyst activity with an increase in the coke deposition. 3.45% of weight loss was detected for Ni_3Co_1 catalyst due to its lower acidity. It was found that 53.5% of phenol conversion and 50.4% of hydrogen yield was achieved with the Ni_3Co_1 catalyst.

Acknowledgement

The authors acknowledge the financial support given for this work by Universiti Teknologi Malaysia (UTM) under the Research University Grant (10H19 and 13H36) and The Malaysian Ministry of Higher Education under FRGS 4F403.

REFERENCES

[1] Shokrollahi Yancheshmeh M, Radfarnia HR, Iliuta MC. High temperature CO_2 sorbents and their application for hydrogen production by sorption enhanced steam reforming process. Chem Eng J 2016;283:420–44.
[2] Nabgan B, Moghadamian K, Tuan Abdullah TA, Nabgan W, Saeh I. Glycerol steam reforming for production of hydrogen ethylene and ethane: thermodynamic Analysis. Int J Environ Res Clean Energy 2016;2:9–11.
[3] Hafizi A, Rahimpour MR, Hassanajili S. Hydrogen production via chemical looping steam methane reforming process: effect of cerium and calcium promoters on the performance of Fe_2O_3/Al_2O_3 oxygen carrier. Appl Energy 2016;165:685–94.
[4] Dang C, Yu H, Wang H, Peng F, Yang Y. A bi-functional Co–CaO–$Ca_{12}Al_{14}O_{33}$ catalyst for sorption-enhanced steam reforming of glycerol to high-purity hydrogen. Chem Eng J 2016;286:329–38.
[5] Abdullah TAT, Nabgan W, Kamaruddin MJ, Mat R, Johari A, Ahmad A. Hydrogen production from acetic acid steam reforming over bimetallic Ni-Co on La_2O_3 catalyst - effect of the catalyst dilution. Appl Mech Mater 2014;493:39–44.
[6] Xie H, Yu Q, Yao X, Duan W, Zuo Z, Qin Q. Hydrogen production via steam reforming of bio-oil model compounds over supported nickel catalysts. J Energy Chem 2015;24:299–308.
[7] Tande LN, Dupont V. Autothermal reforming of palm empty fruit bunch bio-oil: thermodynamic modelling. AIMS Energy 2016;4:68–92.
[8] Naik SN, Goud VV, Rout PK, Dalai AK. Production of first and second generation biofuels: a comprehensive review. Renew Sustain Energy Rev 2010;14:578–97.
[9] Bu Q, Lei H, Ren S, Wang L, Holladay J, Zhang Q, et al. Phenol and phenolics from lignocellulosic biomass by catalytic microwave pyrolysis. Bioresour Technol 2011;102:7004–7.
[10] Kechagiopoulos PN, Voutetakis SS, Lemonidou AA, Vasalos IA. Hydrogen production via steam reforming of the aqueous phase of bio-oil in a fixed bed reactor. Energy Fuels 2006;20:2155–63.
[11] Wang Z, Pan Y, Dong T, Zhu X, Kan T, Yuan L, et al. Production of hydrogen from catalytic steam reforming of bio-oil using C12A7-O^--based catalysts. Appl Catal A General 2007;320:24–34.
[12] Garbarino G, Sanchez Escribano V, Finocchio E, Busca G. Steam reforming of phenol–ethanol mixture over 5% Ni/Al_2O_3. Appl Catal B Environ 2012;113–114:281–9.
[13] Constantinou DA, Efstathiou AM. Low-temperature purification of gas streams from phenol by steam reforming over novel supported-Rh catalysts. Appl Catal B Environ 2010;96:276–89.
[14] Polychronopoulou K, Costa CN, Efstathiou AM. The role of oxygen and hydroxyl support species on the mechanism of H_2 production in the steam reforming of phenol over metal oxide-supported-Rh and -Fe catalysts. Catal Today 2006;112:89–93.
[15] Nabgan W, Tuan Abdullah T, Mat R, Nabgan B, Gambo Y, Johari A. Evaluation of reaction parameters of the phenol steam reforming over Ni/Co on ZrO_2 using the full factorial experimental design. Appl Sci 2016;6:223.
[16] Nabgan W, Saeh I, Tuan Abdullah TA, Nabgan B, Mat R, Gambo Y, et al. An investigation of phenol steam reforming for hydrogen production: thermodynamic analysis. Int J Environ Res Clean Energy 2016;2:1–4.
[17] Polychronopoulou K, Bakandritsos A, Tzitzios V, Fierro JLG, Efstathiou AM. Absorption-enhanced reforming of phenol by steam over supported Fe catalysts. J Catal 2006;241:132–48.
[18] Matas Güell B, Babich IV, Lefferts L, Seshan K. Steam reforming of phenol over Ni-based catalysts – a comparative study. Appl Catal B Environ 2011;106:280–6.
[19] Constantinou DA, Efstathiou AM. The steam reforming of phenol over natural calcite materials. Catal Today 2009;143:17–24.
[20] Nabgan W, Tuan Abdullah TA, Mat R, Nabgan B, Gambo Y, Moghadamian K. Acetic acid-phenol steam reforming for hydrogen production: effect of different composition of La_2O_3-Al_2O_3 support for bimetallic Ni-Co catalyst. J Environ Chem Eng 2016;4:2765–73.
[21] Polychronopoulou K, Fierro JLG, Efstathiou AM. The phenol steam reforming reaction over MgO-based supported Rh catalysts. J Catal 2004;228:417–32.
[22] Constantinou DA, Álvarez-Galván MC, Fierro JLG, Efstathiou AM. Low-temperature conversion of phenol into CO, CO_2 and H_2 by steam reforming over La-containing supported Rh catalysts. Appl Catal B Environ 2012;117–118:81–95.
[23] Constantinou DA, Fierro JLG, Efstathiou AM. The phenol steam reforming reaction towards H_2 production on natural calcite. Appl Catal B Environ 2009;90:347–59.
[24] Rioche C, Kulkarni S, Meunier FC, Breen JP, Burch R. Steam reforming of model compounds and fast pyrolysis bio-oil on supported noble metal catalysts. Appl Catal B Environ 2005;61:130–9.
[25] Bi X, Wang P, Jiang H. Catalytic activity of CuO_n–La_2O_3/γ-Al_2O_3 for microwave assisted ClO_2 catalytic oxidation of phenol wastewater. J Hazard Mater 2008;154:543–9.
[26] Garcia La, French R, Czernik S, Chornet E. Catalytic steam reforming of bio-oils for the production of hydrogen: effects of catalyst composition. Appl Catal A General 2000;201:225–39.
[27] Polychronopoulou K, Giannakopoulos K, Efstathiou AM. Tailoring MgO-based supported Rh catalysts for purification of gas streams from phenol. Appl Catal B Environ 2012;111–112:360–75.

[28] Polychronopoulou K, Costa CN, Efstathiou AM. The steam reforming of phenol reaction over supported-Rh catalysts. Appl Catal A General 2004;272:37–52.

[29] Luisetto I, Tuti S, Di Bartolomeo E. Co and Ni supported on CeO_2 as selective bimetallic catalyst for dry reforming of methane. Int J Hydrogen Energy 2012;37:15992–9.

[30] Vita A, Cristiano G, Italiano C, Pino L, Specchia S. Syngas production by methane oxy-steam reforming on Me/CeO_2 (Me=Rh, Pt, Ni) catalyst lined on cordierite monoliths. Appl Catal B Environ 2015;162:551–63.

[31] Shukla S, Seal S. Thermodynamic tetragonal phase stability in sol–gel derived nanodomains of pure zirconia. J Phys Chem B 2004;108:3395–9.

[32] Rossetti I, Compagnoni M, Torli M. Process simulation and optimisation of H_2 production from ethanol steam reforming and its use in fuel cells. 1. Thermodynamic and kinetic analysis. Chem Eng J 2015;281:1024–35.

[33] Xu J, Zhou W, Wang J, Li Z, Ma J. Characterization and analysis of carbon deposited during the dry reforming of methane over $Ni/La_2O_3/Al_2O_3$ catalysts. Chin J Catal 2009;30:1076–84.

[34] Darensbourg DJ, Holtcamp MW, Longridge EM, Khandelwal B, Klausmeyer KK, Reibenspies JH. Role of the metal center in the homogeneous catalytic decarboxylation of select carboxylic acids. Copper(I) and zinc(II) derivatives of cyanoacetate. J Am Chem Soc 1995;117:318–28.

[35] Ibrahim S, Al Shoaibi A, Gupta AK. Toluene destruction in thermal stage of Claus reactor with oxygen enriched air. Appl Energy 2014;115:1–8.

[36] Rajagopal K, Lacerda R, Slobodcicov I, Campagnolo E. Modeling and simulation of hydrogen sulfide removal from petroleum production lines by chemical scavengers. Chem Eng Commun 2009;196:1237–48.

[37] Hu X, Lu G. Acetic acid steam reforming to hydrogen over $Co–Ce/Al_2O_3$ and $Co–La/Al_2O_3$ catalysts—The promotion effect of Ce and La addition. Catal Commun 2010;12:50–3.

[38] Nabgan W, Abdullah TAT, Mat R, Nabgan B, Jalil AA, Firmansyah L, et al. Production of hydrogen via steam reforming of acetic acid over Ni and Co supported on La_2O_3 catalyst. Int J Hydrogen Energy 2016. http://dx.doi.org/10.1016/j.ijhydene.2016.04.176 [In Press].

[39] Chen L, Zhu Q, Hao Z, Zhang T, Xie Z. Development of a Co–Ni bimetallic aerogel catalyst for hydrogen production via methane oxidative CO_2 reforming in a magnetic assisted fluidized bed. Int J Hydrogen Energy 2010;35:8494–502.

[40] Takanabe K, Nagaoka K, Nariai K, Aika K-i. Titania-supported cobalt and nickel bimetallic catalysts for carbon dioxide reforming of methane. J Catal 2005;232:268–75.

[41] Djinović P, Osojnik Črnivec IG, Erjavec B, Pintar A. Influence of active metal loading and oxygen mobility on coke-free dry reforming of Ni–Co bimetallic catalysts. Appl Catal B Environ 2012;125:259–70.

[42] Feng T-C, Zheng W-T, Sun K-Q, Xu B-Q. CO_2 reforming of methane over coke-resistant $Ni–Co/Si_3N_4$ catalyst prepared via reactions between silicon nitride and metal halides. Catal Commun 2016;73:54–7.

[43] Zhang J, Wang H, Dalai AK. Development of stable bimetallic catalysts for carbon dioxide reforming of methane. J Catal 2007;249:300–10.

[44] Zhang J, Wang H, Dalai AK. Effects of metal content on activity and stability of Ni-Co bimetallic catalysts for CO_2 reforming of CH_4. Appl Catal A General 2008;339:121–9.

[45] Liu W-w, Wang X-p, Hu C-w, Tong D-m, Zhu L-f, Li G-y. Catalytic pyrolysis of distillers dried grain with solubles: an attempt towards obtaining value-added products. Int J Hydrogen Energy 2014;39:6371–83.

[46] Osorio-Vargas P, Campos CH, Navarro RM, Fierro JLG, Reyes P. $Rh/Al_2O_3–La_2O_3$ catalysts promoted with CeO_2 for ethanol steam reforming reaction. J Mol Catal A Chem 2015;407:169–81.

[47] Ning P, Song Z, Li H, Zhang Q, Liu X, Zhang J, et al. Selective catalytic reduction of NO with NH_3 over $CeO_2–ZrO_2–WO_3$ catalysts prepared by different methods. Appl Surf Sci 2015;332:130–7.

[48] Nabgan W, Tuan Abdullah TA, Mat R, Nabgan B, Triwahyono S, Ripin A. Hydrogen production from catalytic steam reforming of phenol with bimetallic nickel-cobalt catalyst on various supports. Appl Catal A General 2016;527:161–70.

[49] Zhao X, Lu G. Modulating and controlling active species dispersion over Ni–Co bimetallic catalysts for enhancement of hydrogen production of ethanol steam reforming. Int J Hydrogen Energy 2016;41:3349–62.

[50] Li W, Zhao Z, Ding F, Guo X, Wang G. Syngas production via steam–CO_2 dual reforming of methane over LA-Ni/ZrO_2 catalyst prepared by l-arginine ligand-assisted strategy: enhanced activity and stability. ACS Sustain Chem Eng 2015;3:3461–76.

[51] Zhang G, Su A, Zhao Y. Synthesis of ZrO_2-based catalyst for coke oven gas CO shift via an orthogonal experiment design. Synth React Inorg Metal-Organic Nano-Metal Chem 2016;46:91–4.

[52] Xie H, Lu J, Shekhar M, Elam JW, Delgass WN, Ribeiro FH, et al. Synthesis of Na-Stabilized nonporous t-ZrO_2 supports and Pt/t-ZrO_2 catalysts and application to water-gas-shift reaction. ACS Catal 2013;3:61–73.

[53] Mguni LL. Biodiesel production over supported nano-magnesium oxide particles. University of Johannesburg; 2012.

[54] Fatsikostas AN, Kondarides DI, Verykios XE. Production of hydrogen for fuel cells by reformation of biomass-derived ethanol. Catal Today 2002;75:145–55.

[55] García-Lario AL, Grasa GS, Murillo R. Performance of a combined CaO-based sorbent and catalyst on H_2 production, via sorption enhanced methane steam reforming. Chem Eng J 2015;264:697–705.

[56] Martavaltzi CS, Lemonidou AA. Hydrogen production via sorption enhanced reforming of methane: development of a novel hybrid material—reforming catalyst and CO_2 sorbent. Chem Eng Sci 2010;65:4134–40.

[57] Mi Y, Yuan D, Liu Y, Zhang J, Xiao Y. Synthesis of hexagonal close-packed nanocrystalline nickel by a thermal reduction process. Mater Chem Phys 2005;89:359–61.

[58] Beach ER, Shqau K, Brown SE, Rozeveld SJ, Morris PA. Solvothermal synthesis of crystalline nickel oxide nanoparticles. Mater Chem Phys 2009;115:371–7.

[59] Ingersoll JC, Mani N, Thenmozhiyal JC, Muthaiah A. Catalytic hydrolysis of sodium borohydride by a novel nickel–cobalt–boride catalyst. J Power Sources 2007;173:450–7.

[60] Li Y, Wang R, Qi F, Wang C. Preparation, characterization and microwave absorption properties of electroless Ni–Co–P-coated SiC powder. Appl Surf Sci 2008;254:4708–15.

[61] Cabo M, Garroni S, Pellicer E, Milanese C, Girella A, Marini A, et al. Hydrogen sorption performance of MgH_2 doped with mesoporous nickel- and cobalt-based oxides. Int J Hydrogen Energy 2011;36:5400–10.

[62] Han SJ, Bang Y, Yoo J, Seo JG, Song IK. Hydrogen production by steam reforming of ethanol over mesoporous $Ni–Al_2O_3–ZrO_2$ xerogel catalysts: effect of nickel content. Int J Hydrogen Energy 2013;38:8285–92.

[63] Lin SSY, Kim DH, Ha SY. Metallic phases of cobalt-based catalysts in ethanol steam reforming: the effect of cerium oxide. Appl Catal A General 2009;355:69–77.

[64] Xu J, Zhou W, Li Z, Wang J, Ma J. Biogas reforming for hydrogen production over nickel and cobalt bimetallic catalysts. Int J Hydrogen Energy 2009;34:6646–54.
[65] Alves-Rosa MA, Martins L, Hammer P, Pulcinelli SH, Santilli CV. Sulfated zirconia foams synthesized by integrative route combining surfactants, air bubbles and sol-gel transition applied to heterogeneous catalysis. RSC Adv 2016;6:6686–94.
[66] Mondal T, Pant KK, Dalai AK. Catalytic oxidative steam reforming of bio-ethanol for hydrogen production over Rh promoted Ni/CeO_2–ZrO_2 catalyst. Int J Hydrogen Energy 2015;40:2529–44.
[67] Yasu-eda T, Kitamura S, Ikenaga N-o, Miyake T, Suzuki T. Selective oxidation of alcohols with molecular oxygen over Ru/CaO–ZrO_2 catalyst. J Mol Catal A Chem 2010;323:7–15.
[68] Kumar P, Sun Y, Idem RO. Comparative study of Ni-based mixed oxide catalyst for carbon dioxide reforming of methane. Energy Fuels 2008;22:3575–82.
[69] de Freitas Silva T, Reis CGM, Lucrédio AF, Assaf EM, Assaf JM. Hydrogen production from oxidative reforming of methane on Ni/γ-Al_2O_3 catalysts: effect of support promotion with La, La–Ce and La–Zr. Fuel Process Technol 2014;127:97–104.
[70] Khodakov AY, Chu W, Fongarland P. Advances in the development of novel cobalt Fischer–Tropsch catalysts for synthesis of long-chain hydrocarbons and clean fuels. Chem Rev 2007;107:1692–744.
[71] Luo N, Ouyang K, Cao F, Xiao T. Hydrogen generation from liquid reforming of glycerin over Ni–Co bimetallic catalyst. Biomass Bioenergy 2010;34:489–95.
[72] Koh ACW, Chen L, Kee Leong W, Johnson BFG, Khimyak T, Lin J. Hydrogen or synthesis gas production via the partial oxidation of methane over supported nickel–cobalt catalysts. Int J Hydrogen Energy 2007;32:725–30.
[73] Zhang Y, Liu Z, Ren S, Wang W, Shen B. Study on the basic centers and active oxygen species of solid-base catalysts for oxidation of iso-mercaptans. Appl Catal A General 2014;473:125–31.
[74] Boréave A, Auroux A, Guimon C. Nature and strength of acid sites in HY zeolites: a multitechnical approach. Microporous Mater 1997;11:275–91.
[75] Chen L, Zhu Q, Wu R. Effect of Co–Ni ratio on the activity and stability of Co–Ni bimetallic aerogel catalyst for methane Oxy-CO_2 reforming. Int J Hydrogen Energy 2011;36:2128–36.
[76] Cobo M, Pieruccini D, Abello R, Ariza L, Córdoba LF, Conesa JA. Steam reforming of ethanol over bimetallic RhPt/La_2O_3: long-term stability under favorable reaction conditions. Int J Hydrogen Energy 2013;38:5580–93.
[77] Natesakhawat S, Watson RB, Wang X, Ozkan US. Deactivation characteristics of lanthanide-promoted sol–gel Ni/Al_2O_3 catalysts in propane steam reforming. J Catal 2005;234:496–508.
[78] Yang E-h, Kim NY, Noh Y-s, Lim SS, Jung J-S, Lee JS, et al. Steam CO_2 reforming of methane over $La_{1-x}Ce_xNiO_3$ perovskite catalysts. Int J Hydrogen Energy 2015;40:11831–9.
[79] Gallego GS, Marín JG, Batiot-Dupeyrat C, Barrault J, Mondragón F. Influence of Pr and Ce in dry methane reforming catalysts produced from $La_{1-x}A_xNiO_{3-\delta}$ perovskites. Appl Catal A General 2009;369:97–103.